Assimilation of INSAT-3D imager water vapour clear sky brightness temperature in the NCMRWF's assimilation and forecast system

S Indira Rani[1],*, Ruth Taylor[2], Priti Sharma[1], M T Bushair[1],
Buddhi Prakash Jangid[1], John P George[1] and E N Rajagopal[1]

[1]*National Centre for Medium Range Weather Forecasting (NCMRWF), Ministry of Earth Sciences (MoES), A-50, Sector-62, Noida, Uttar Pradesh 201301, India.*
[2]*Satellite Applications, Met Office, Exeter EX1 3PB, UK.*
Corresponding author. e-mail: indira@ncmrwf.gov.in   ranispl@gmail.com

This paper describes the direct assimilation of water vapour (WV) clear sky brightness temperatures (CSBTs) from the INSAT-3D imager in the National Centre for Medium Range Weather Forecasting (NCMRWF) Unified Model (NCUM) assimilation and forecast system. INSAT-3D imager WV CSBTs show a systematic bias of 2–3 K compared to the data simulated from the model first guess fields in the pre-assimilation study. The bias in the INSAT-3D imager WV CSBTs is removed using a statistical bias correction prior to assimilation. The impact of INSAT-3D imager WV channel CSBTs is investigated through different approaches: (i) single observation experiments and (ii) global assimilation experiments using the hybrid-four-dimensional variational technique. Single observation experiments of channels of the same frequency from different instruments like the INSAT-3D imager and sounder, and the Meteosat visible and infrared imager (MVIRI) onboard Meteosat-7, show the INSAT-3D imager and MVIRI WV channels have a similar impact on the analysis increment. Global assimilation clearly shows the positive impact of the INSAT-3D imager WV CSBTs on the humidity and upper tropospheric wind fields, whereas the impact on the temperature field, particularly over the tropics, is neutral. Validation of model forecasted parameters with the in situ radio sonde observations also showed the positive impact of assimilation on the humidity and wind fields. INSAT-3D imager WV CSBTs have been assimilated operationally in NCUM since August 2018.

Keywords. INSAT-3D; WV; CSBT; hybrid-4DVAR; NCUM; NWP.

1. Introduction

The primary use of radiance products from geostationary imagers is the derivation of atmospheric motion vectors (AMVs) (Deb *et al.* 2015 and references therein). AMVs are produced by tracking features in successive images in visible, infrared (IR) and water vapour (WV) channels.

The National Centre for Medium Range Weather Forecasting (NCMRWF) assimilates AMVs from different geostationary satellites including INSAT-3D and polar satellites in its operational numerical weather prediction (NWP) models (Das Gupta *et al.* 2015; Sharma *et al.* 2016). WV-channel derived winds are of two types: clear and cloudy. The clear sky WV winds are derived by

tracking the features of clear sky moisture. As the radiation in the WV channel under clear sky conditions is emitted from a deep atmosphere, height assignment is seldom problematic (Velden *et al.* 1997). Large errors will creep into the assimilation system if both cloudy and clear WV winds are considered together (Rao *et al.* 2002; Rani and Das Gupta 2014). Direct assimilation of clear-sky WV radiances is an alternative method to make the fullest use of the WV-channel information from geostationary satellite imagers.

There are many reported studies on clear sky brightness temperature (CSBT) assimilation from both geostationary and polar satellites in the operational and research environments. Assimilation of humidity-sensitive data from different polar orbiting platforms, as well as from a number of geostationary platforms at the European Centre for Medium Range Weather Forecasting (ECMWF) is detailed in Thepaut (2003) and Kopken *et al.* (2004). Trigo and Viterbo (2003) provide a comparison between the clear sky window channel radiances and the ECMWF model. Assimilation of Meteosat clear sky radiances within the four-dimensional variational (4DVAR) system at ECMWF with details of data quality monitoring, bias correction and single cycle experiments are detailed in Munro *et al.* (2004). Szyndel *et al.* (2005) described the addition of WV sensitive channels from spinning enhanced visible and infrared imager (SEVIRI) from Meteosat-8 to the ECMWF system. The assimilation of SEVIRI CSBTs in a high resolution limited area model shows that the impacts are confined primarily to the mid- and upper tropospheric humidity fields (Stengel 2008). Singh *et al.* (2010) reported that the assimilation of Kalpana Clear sky WV radiances in the Weather Research Forecast (WRF) system shows a positive impact on the mid- and upper-tropospheric moisture and temperature. Positive forecast impacts from assimilating GOES imager radiances were seen when verified against different types of airborne and station observations (Yang *et al.* 2017). Kurzrock *et al.* (2018) reviewed the use of geostationary satellite observations in regional-scale models for short-term cloud forecasting applications. Assimilation of Himawari-8 radiances improved the analysed cyclone structure and intensity (Honda *et al.* 2018). Kelkar (2019) provides the story of satellite meteorology in India, its growth and future.

Validation of INSAT-3D sounder and imager radiances shows the quality is similar to that of

other geostationary satellites (Rani and Prasad 2013; Rani *et al.* 2016). Kumar *et al.* (2016) illustrated the impact of INSAT-3D winds in the WRF model. Singh *et al.* (2016) demonstrated that the assimilation of temperature and WV sensitive radiances from the INSAT-3D sounder and imager improved not only the temperature and humidity fields but the wind field as well. Rani *et al.* (2016) reported the near neutral impact of INSAT-3D sounder radiance assimilation in the UK Met Office Unified Model assimilation and the forecast system.

This study demonstrates the impact of CSBTs from the INSAT-3D imager WV channel in the NCMRWF Unified Model (NCUM) hybrid-4DVAR assimilation system through a series of single observation experiments and global assimilation experiments. A brief description of the NCUM assimilation system is provided in section 2. Salient features of the INSAT-3D imager instrument is provided in section 3. Before assimilating, the observed CSBTs are compared with those simulated from the model background. The bias in the observed brightness temperatures with respect to the model-simulated brightness temperature is calculated prior to the assimilation. The bias correction method applied for the WV CSBTs and the comparison of observed, simulated and corrected brightness temperatures are described in section 4. The results of the single observation experiment, the global assimilation experiments and validation of the forecast fields against in situ radiosonde observations are discussed in section 5, and the conclusions are listed in section 6.

2. The NCUM assimilation system

The NCUM NWP system is adapted from the unified model assimilation-forecast system of 'UM Partnership' (Rajagopal *et al.* 2012; George *et al.* 2016; Kumar *et al.* 2018). The seamless modelling approach of the UM allows the use of the same dynamical core and parametrisation schemes across a broad range of spatial and temporal scales. Different components of the NCUM are (i) observation pre-processing system (OPps), (ii) observation processing system (OPS), (iii) hybrid-4DVAR assimilation system, (iv) surface data assimilation system (SURF) and (v) the unified model. NCMRWF receives global observations from different sources and figure 1 shows the
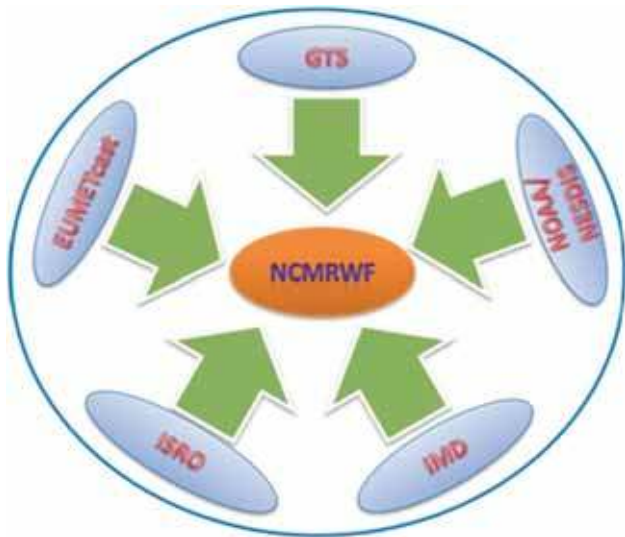
Figure 1. Meteorological data reception at NCMRWF.

Figure 2. Weighting function of INSAT-3D imager channels.

block diagram of global data reception at NCMRWF. OPps does pre-processing of different observation types received at NCMRWF and converts the data into the required format that the OPS can read (Prasad 2012, 2014; Prasad and Rani 2014). The OPS does processing and different quality control of observations and produces the required inputs for the hybrid-4DVAR assimilation system.

Variational data assimilation methods use model fields to define the structure of background and forecast errors. These background and forecast errors along with the description of observation errors are the main inputs to an iterative algorithm to find the best analysis using available observations. Variational data assimilation techniques are ideal for dense observations from satellite and radars. 4DVAR data assimilation had/has been used by most of the main global NWP centres for more than a decade (Rabier 2005). The 4DVAR was implemented in the unied system (UM) in 2004 (Rawlins *et al.* 2007). A weakness of the basic 4DVAR method is it uses a fixed 'climatological' model of the error covariance in the background forecast, which lacks the flow-dependent error of the day (Lorenc 2003a). Lorenc (2003b) reviewed the ensemble Kalman filter (EnKF) methods and compared them to the 4DVAR assimilation method. This study revealed that the EnKF is attractive when building a new medium-range ensemble NWP system, but less suitable for NWP systems with uncertainty in a wide range of scales; it may not use high-resolution satellite data as effectively as 4DVAR. To address
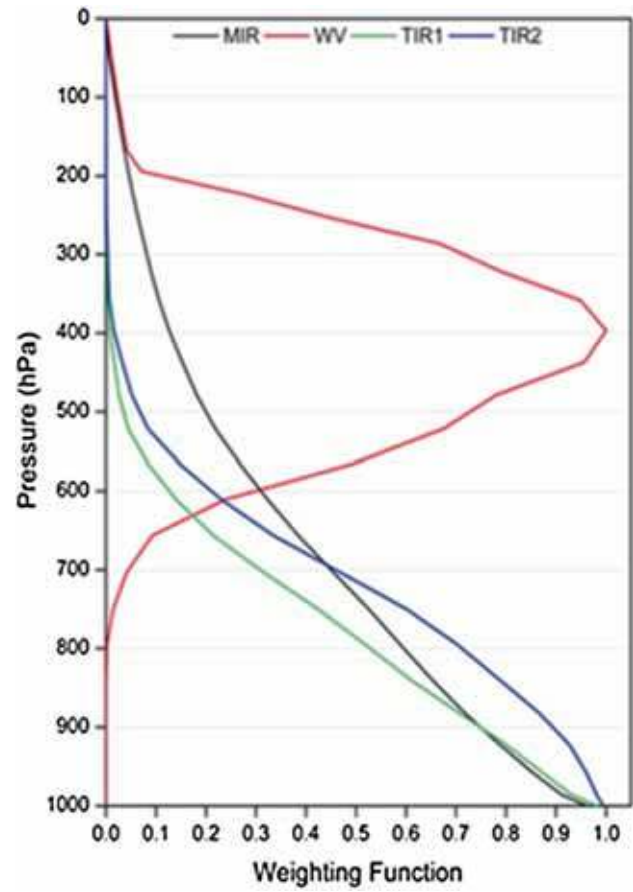
this, the day-to-day variation of flow-dependent errors in the UM system, Clayton *et al.* (2013) introduced a 'hybrid-4DVAR' method. The term 'hybrid' in the hybrid-4DVAR method refers to the combination of a climatological covariance model with covariances calculated from an ensemble of forecasts, which are designed to sample the current uncertainty.

NCMRWF runs an ensemble system based on NCUM. The hybrid-4DVAR assimilation system combines flow-dependent errors from the ensemble members and climatological errors (Clayton *et al.* 2013; Lorenc *et al.* 2015). A dual resolution 4DVAR approach is used in the variational assimilation system: a low resolution configuration of 60 km horizontal resolution with 30 iterations and thereafter a high resolution configuration of 40 km horizontal resolution with 40 iterations. The variational assimilation system combines observations and first guesses and produces the analysis for the forecast model. The SURF system produces surface data analysis. More details of the NCUM version used in this study are available in George *et al.* (2016).
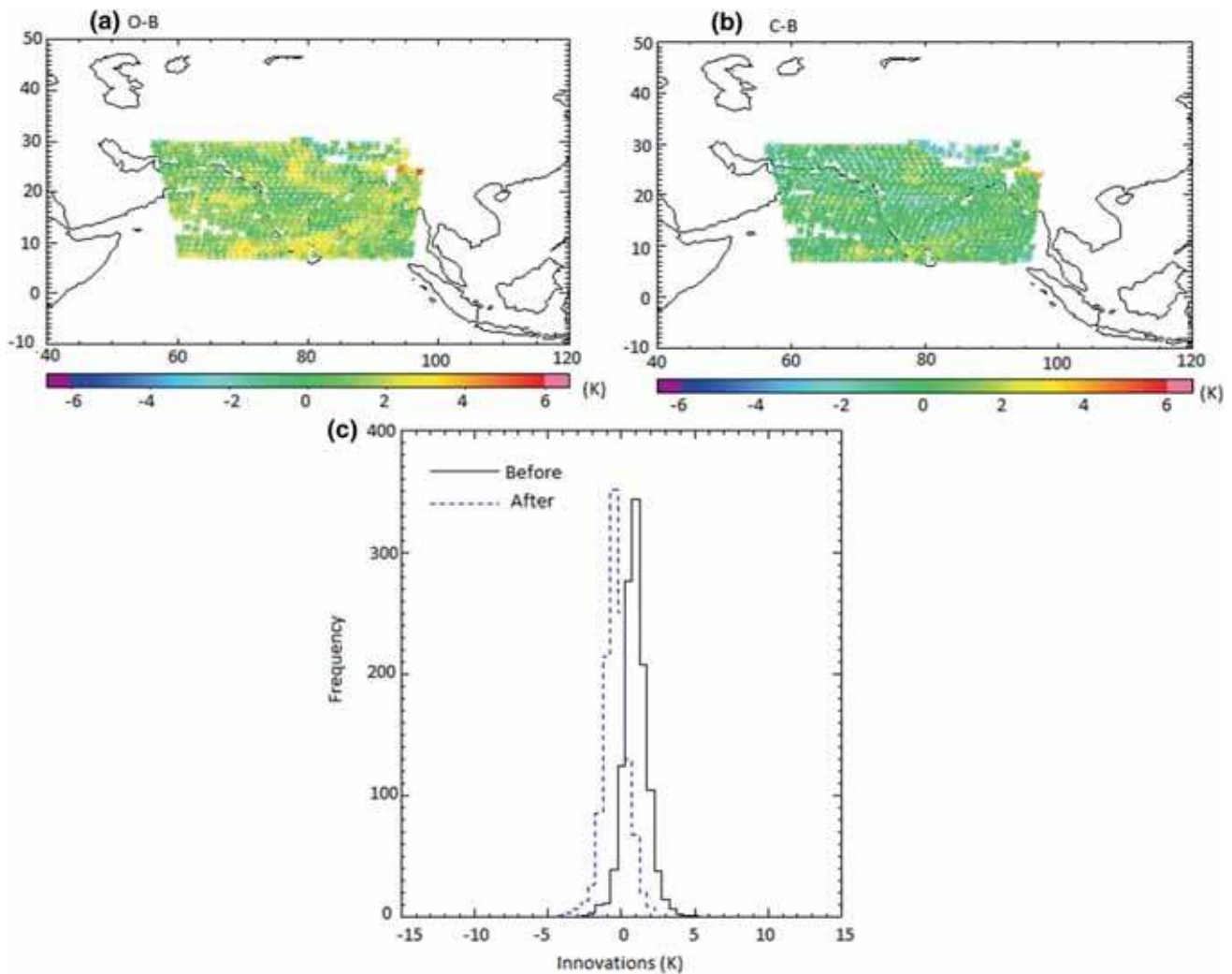
Figure 3. Innovations without and with bias correction for the INSAT-3D imager WV channel: (**a**) spatial plot of observation–background (O–B), (**b**) spatial plot of corrected observation–background (C–B) and (**c**) the distribution of innovations without and with bias correction.

3. The INSAT-3D imager instrument

After GOES, INSAT-3D is the second satellite of its kind and the first over India and surrounding oceanic regions. The main meteorological payloads onboard INSAT-3D are the imager with six channels and the sounder with 19 channels. The channels of the INSAT-3D imager are distributed in the visible and IR region of the spectrum with the Earth's full disc imaging capability. The visible imager channel operates in 0.52–0.72 μm and provides information during day time. The short wave infrared (SWIR) (1.55–1.70 μm), mid-wave infrared (MIR) (3.80–4.00 μm), WV (6.50–7.00 μm) and two split thermal infrared (TIR) channels provide atmospheric information both day and night. The split TIR channels operate in 10.2–11.2 μm (TIR-1) and 11.5–12.5 μm (TIR-2). Both visible and SWIR have

a ground resolution of 1 km at the sub-satellite point. The split TIR channels and the MIR channel have 4 km ground resolution, whereas the WV channel is sampled every 8 km.

Figure 2 shows the weighting function of INSAT-3D imager channels. From figure 2, it can be seen that WV channel peaks high in the atmosphere and the surface impact is less compared to the other three channels. WV and high clouds absorb the radiation in this spectral region so that the surface of the earth and low clouds are nearly obscured in WV images. Moreover, WV radiance provides valuable information to NWP, particularly, over the upper tropospheric levels of the atmosphere, where there are fewer AMVs. Only the WV radiances from the INSAT-3D imager are assimilated in the NCUM system; other channels are not used.
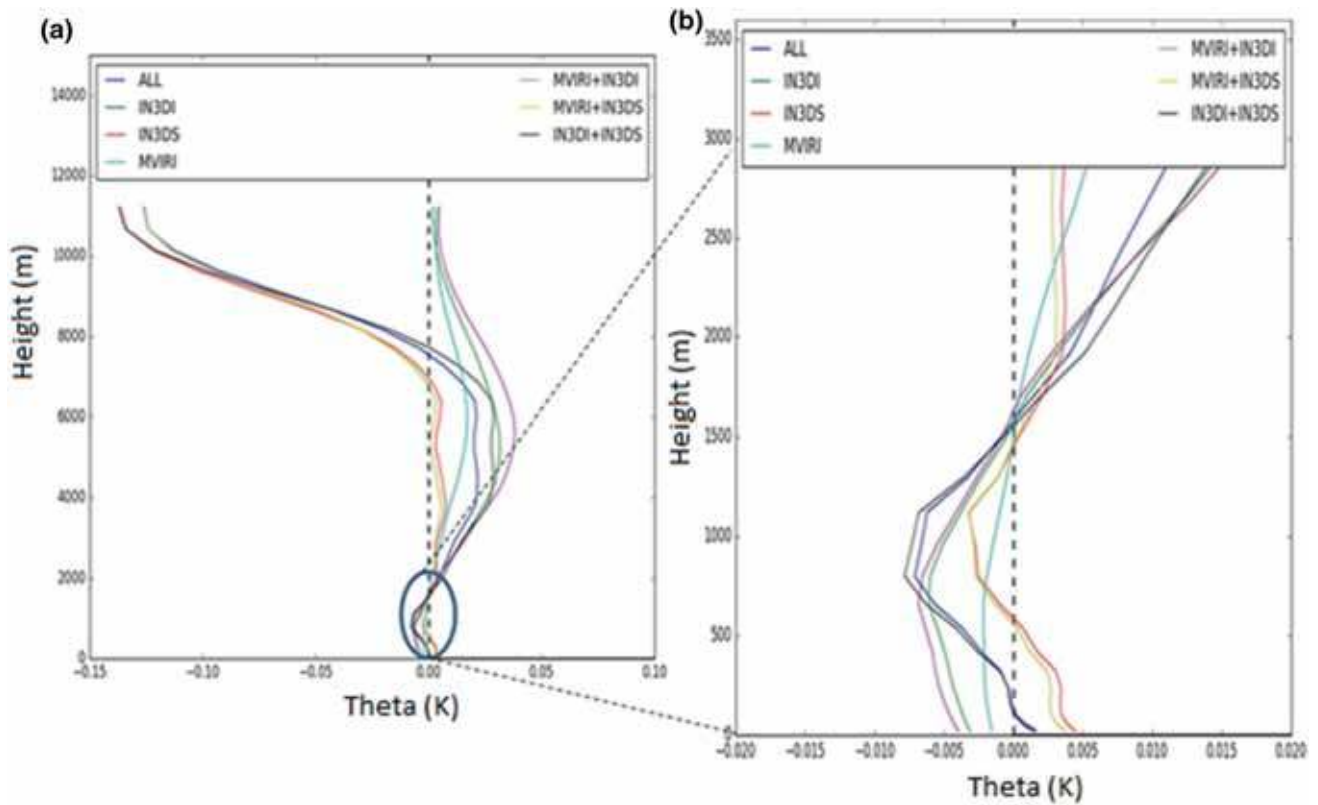
Figure 4. Analysis increment in theta (K) from single observation experiment: (**a**) from surface to 12 km and (**b**) zoomed profile in the lower region up to 3 km.

4. Bias correction

Satellite instruments do not measure temperature, wind or humidity, which are the main prognostic variables in the numerical model-governing equations. What satellite instruments measure is the radiance that reaches the top of the atmosphere at a given frequency and this radiance is related to atmospheric conditions like temperature, humidity, winds, clouds, chemical constitutions, etc. Radiative transfer (RT) equations are used (i) to convert the temperature and humidity profiles to radiance, the forward problem and (ii) the radiance to estimate geophysical parameters like temperature, humidity, etc., the inverse problem. Before assimilating the radiances (as brightness temperatures) in NWP models, the satellite measured radiances have to be bias corrected. An RT model calculates the model brightness temperature using model temperature and humidity profiles, and the satellite measured brightness temperatures are compared with these equivalents computed from the NWP model. In assimilation, the assumptions made are (i) the RT model is perfect, (ii) the observed satellite radiances are free of calibration errors and (iii) the NWP model is free from systematic errors. In practice, these

assumptions are not always valid; all three produce biases which vary with time, geography, air mass, scan position of satellite instrument and the position of the satellite around its orbit (Bell *et al.* 2008; Lu *et al.* 2011; Doherty *et al.* 2015).

In this study, the model equivalents of the observed CSBTs are computed using RTTOV version-9 (Saunders *et al.* 2010). The differences between the observations (O) and the simulations (B) are known as innovations (O–B). Innovations are used to diagnose the errors in the observations and to calculate a bias correction. Bias correction methods can be of different types, static and adaptive, irrespective of the data assimilation schemes. A static bias correction scheme is adopted in this study. The data were bias corrected following the method of Harris and Kelly (2001), using 850–300 hPa thickness, 200–50 hPa thickness and total column water vapour as predictors. Data with more than 30% of a segment cloudy were rejected, as were data with a local satellite zenith angle of 60° or greater and data from a point over ground higher than 1.5 km. In this scheme roughly 1 month data are required to fit the bias correction and the bias correction is updated infrequently, at every 6–12-month interval, or if there has been a

significant change in the bias seen through observation monitoring. In contrast to the statistic bias correction, the variational bias correction (adaptive bias correction) is more effective mainly because the bias correction is continuously updated as part of the main assimilation (Auligne *et al.* 2007), which has been implemented as operational at NCMRWF very recently. The period of study is approximately 15 days and during this short time there may not be a drastic change in the biases in different channels and a static bias correction works effective for this short time span.

Innovations are calculated from the model simulated brightness temperatures and observations and are used for the calculation of biases in the observations. Figure 3(a and b), respectively, shows the spatial plots of the differences between observations and corrected observations from the background. The difference between the observation and background (O–B) reduced after bias correction as seen from figure 3(b), as the difference between the corrected observation and background (C–B). After bias correction, the innovations reduced considerably.

Both the observations and background are assumed to be normally distributed in variational data assimilation. The mean of the innovation distribution shifts towards zero, if the bias correction works properly. Figure 3(c) shows the innovations with and without applying bias correction for the WV channel of the INSAT-3D imager. It can be noted from figure 3(c) that after applying bias correction (dotted curve), the mean of the O–B distribution shifted towards zero, ensuring that the bias correction is working effectively. A bias of 2–3 K is noted in the observed CSBTs in comparison with those simulated from the model background fields using the RT model. The bias corrected observations are assimilated in the NCUM system.

5. Results and discussion

5.1 *Single observation experiments*

Single observation experiments reveal the effect of assimilating single (real) observations from different instruments on humidity and temperature
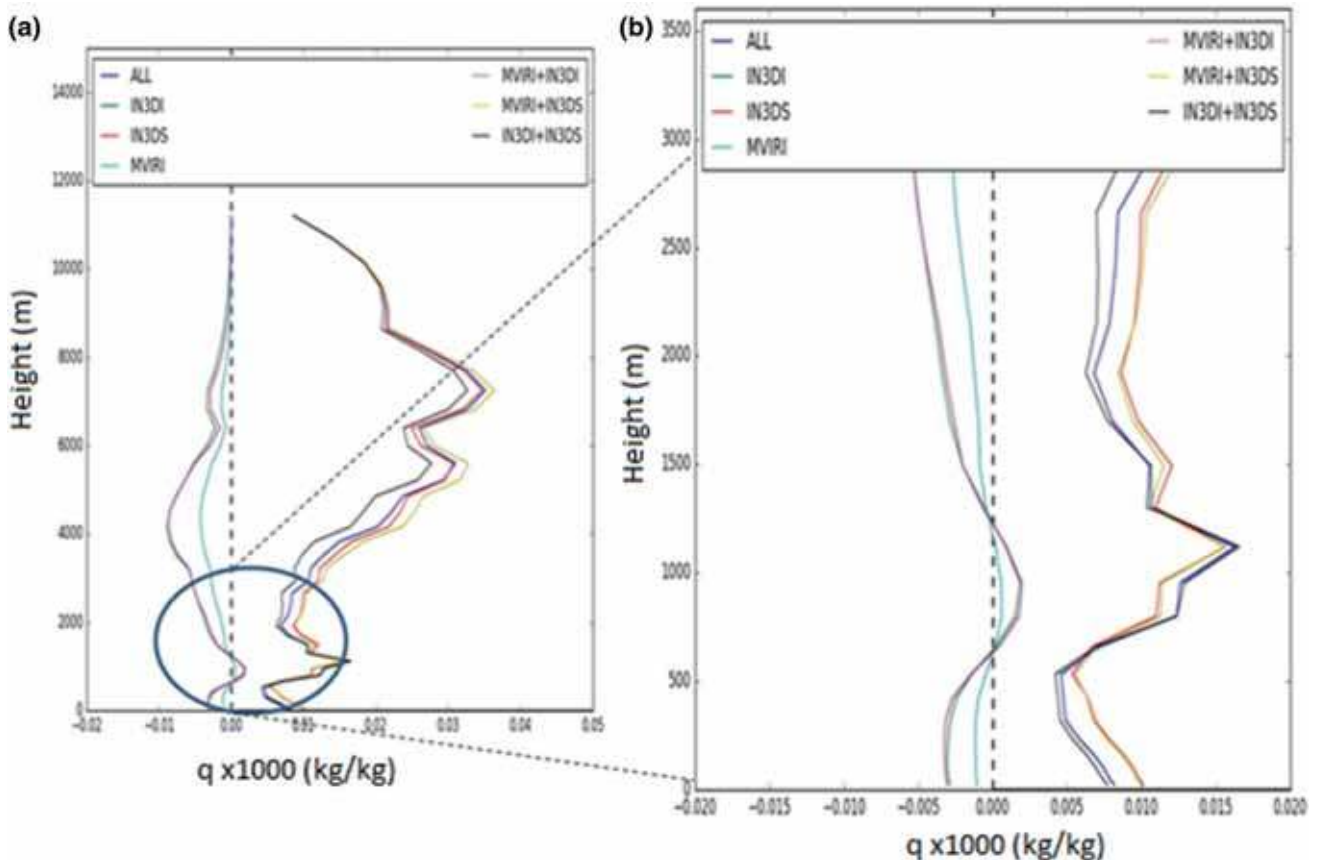

Figure 5. Analysis increment in specific humidity (1000 × kg/kg) from single observation experiments: (**a**) from surface to 12 km and (**b**) zoomed profile in the lower region up to 3 km.

increments. Single observation experiments were carried out for the WV channels of the INSAT-3D imager and the Meteosat visible and infrared imager (MVIRI) onboard the Meteosat-7 satellite, and also the similar wavelength (6.51 μm) channel of the INSAT-3D sounder. The specific aim was to investigate the behaviour of analysis increments due to the imager channel and sounder channel assimilation. In these experiments, all other satellite and conventional data were removed from the assimilation system of NCUM and a single collocated observation from INSAT-3D imager WV channel, MVIRI WV channel and INSAT-3D sounder 6.51 μm channel were assimilated individually. In additional experiments, different combinations of collocated observations from the above three instruments at a single location were assimilated together. The analysis increment at the location of the observation was analysed to examine the impact of each instrument individually and all instruments were combined.

The analysis increment reveals how an observation modifies the background by making use of the error covariance information provided. The increments are made in horizontal as well as vertical directions although the effect is restricted to a limited distance by localisation schemes. Figure 4 shows the potential temperature (theta) increment from the assimilation of a single observation from an INSAT-3D imager WV channel (IN3DI), INSAT-3D sounder 6.51 μm (IN3DS), MVIRI WV channel (MVIRI), combination of imagers (MVIRI + IN3DI) and the combination of imagers and sounder (MVIRI + IN3DS, IN3DI + IN3DS, MVIRI + IN3DI + IN3DS (ALL)). Figure 4(a) depicts the analysis increment in theta due to the assimilation of single observations from different instruments individually and in combination from the surface to a model height of around 12 km. Figure 4(b) is similar to figure 4(a) but the height is limited to 3.0 km, the zoomed out lower part of figure 4(a).
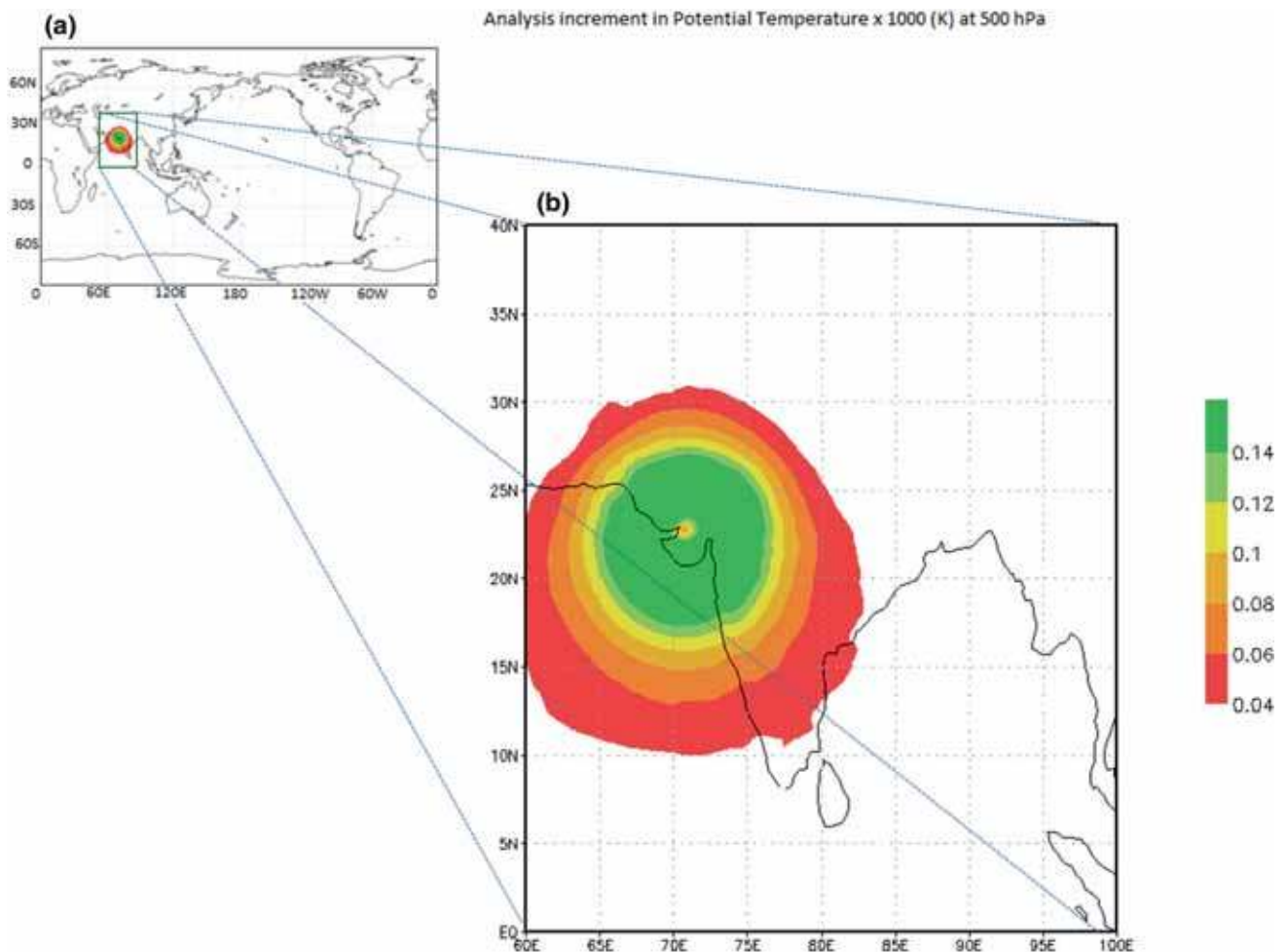

Figure 6. Spatial plot of analysis increment in theta (K) at 500 hPa from single observation experiment (**a**) global domain and (**b**) zoomed over the single observation location and the adjacent area.
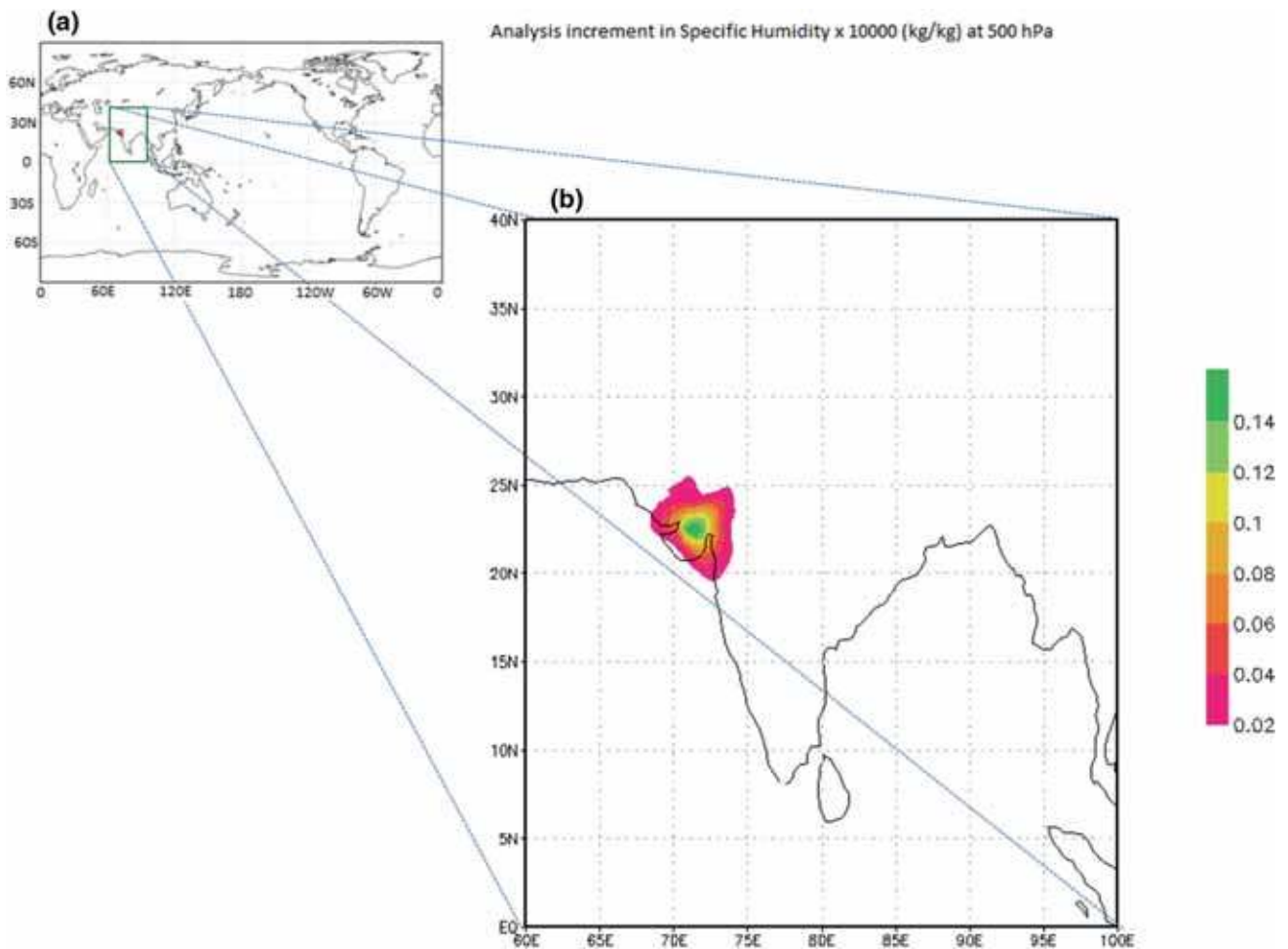
Figure 7. Spatial plot of analysis increment in specific humidity (kg/kg) at 500 hPa from single observation experiment (**a**) global domain and (**b**) zoomed over the single observation location and adjacent area.

In general, the trend in the theta increment is similar for individual instruments and in combination, but a close examination shows that in the lower levels, the imagers (IN3DI, MVIRI, and IN3DI+MVIRI) have a cooling effect up to a model atmospheric height of 1.5 km, whereas the sounder has a heating effect in the lower regions, approximately at 500 m, and thereafter a cooling effect up to 1.5 km (figure 4b). Similar effects to that of the sounder radiance are noticed in the combination of imager and sounder experiments (MVIRI + IN3DS, IN3DI + IN3DS, and MVIRI + IN3DI + IN3DS). Above 1.5 km, the imagers, sounder and the combinations showed a similar impact in theta increment up to a model height of 8 km (figure 4a). Beyond 8 km, imagers have a heating effect whereas the addition of the sounder produces a cooling effect in the model atmosphere. Thus in the temperature increment, both the imagers and sounder have a similar effect, except in the lower levels of the model atmosphere and above 8 km.

The humidity increments from single observation experiments are shown in figure 5(a and b). Figure 5(a) shows the humidity increments from the single observation experiments for different instruments individually and combined from the model surface to a height of ∼12 km, whereas figure 5(b) is the zoomed lower part from figure 5(a). The imagers show a drying effect in the analysis increment; however, the addition of sounder radiances shows a moistening effect throughout, from the surface to a model atmosphere height of approximately 10–11 km. A close examination of the analysis increment in humidity in the lower levels, up to 3 km (figure 5b) shows the moistening effect of imagers between 0.5 and 1.5 km. It is noted from figure 5(a and b) that the humidity increment is driven by sounder radiances, but the addition of imager radiances modifies it. This implies that the sounder radiance has a moistening effect in the analysis increment (red curve), but when imager radiances are added, the

Table 1. *Observations assimilated in the baseline experiment.*

Observation type	Observation description
AHIClear	Advanced Himawari imager radiances from Himawari-8
Aircraft	Upper-air wind and temperature from aircraft
AIRS	Atmospheric infrared sounder of Aqua
AMSR	Radiances from AMSR-2 onboard GCOM satellite
ATOVS	AMSU-A, AMSU-B/MHS, HIRS from NOAA-18 and19, MetOp-A and B
ATMS	Advanced technology microwave sounder in NPP satellite
CrIS	Cross-track infrared sensor observations in NPP satellite
GOESClear	Cloud clear imager radiances from GOES
GPSRO	Global positioning system radio occultation observations from various satellites
GroundGPS	Ground-based GPS observations from various locations
IASI	Infrared atmospheric sounding interferometer from MetOp-A and B
MTSAPHIR	SAPHIR microwave radiances from Megha-Tropiques
Satwind	AMVs from various geostationary and polar orbiting satellites
Scatwind	Advanced scatterometer in MetOp-A and B, ScatSat-1, WindSat
SEVIRIClear	Cloud clear observations from SEVIRI of METEOSAT 11
Sonde	Radiosonde observations, upper-air wind profile from pilot balloons, wind profiles, VAD wind observation from Indian DWR
Surface	Surface observations from land and ocean
SSMIS	SSMIS radiances

moistening effect is decreased (MVIRI + IN3DS (yellow curve), IN3DI + IN3DS (black curve), MVIRI + IN3DI + IN3DS (blue curve) in figure 5(a and b).

From figures 4 and 5, it can be seen that the observation at a given level generates increments all the way to the tropopause/upper tropospheric height. This is due to the characteristics of the weighting function of the particular channel from which the data is assimilated. From figure 2, it can be seen that the INSAT-3D imager WV channel peaks at ~ 400 hPa and this leads to the generation of analysis increment throughout the atmospheric column. The single observation experiments show that the INSAT-3D imager and MVIRI WV channel radiances have a similar influence on the analysis increment of both theta and specific humidity. The vertical structure of specific humidity increment implies that in this case the humidity is driven by the sounder observations in the assimilation system, but the imagers modify it. The analysis increments of both theta and specific humidity show imager WV channels having a similar impact, with more features in the lower model levels.

Figures 4 and 5 show the analysis increment in potential temperature and specific humidity in the vertical. The observations have influence in the horizontal as well. Figures 6 and 7 show the analysis increment in potential temperature and specific humidity at 500 hPa from the single observation experiment where INSAT-3D imager WV CSBT is assimilated at a single point. Both the variables show the spatial extent from the assimilation point and this can be attributed to the flow-dependent features of analysis increment variables. The changes in the potential temperature increment are quite higher than that of specific humidity.

5.2 *Global assimilation experiments: Impact on the NCUM analysis and forecast system*

After confirming the impact of the INSAT-3D imager WV channel on the analysis is similar to that of MVIRI through a set of single observation experiments, the INSAT-3D WV CSBTs were assimilated in the NCUM global assimilation and forecast system. Before the operational production of INSAT-3D imager CSBTs at the Space Application Centre (SAC), Indian Space Research Association (ISRO), SAC provided 15 days of data (1–15 February 2017) to NCMRWF to test in the NCUM assimilation system. Successive 6 hourly assimilations were carried out starting from 00 UTC, 1 February 2017 to 15 February 2017, with four assimilation cycles per day, at 00, 06, 12 and 18 UTCs. The CSBT product is at a horizontal resolution of 50 km. Five days of forecasts were prepared based on daily 00 UTC initial conditions.

This section discusses the impact of INSAT-3D imager WV radiances on forecast fields such as temperature, humidity and winds. Two assimilation experiments were set up, such that one assimilates all the conventional and satellite
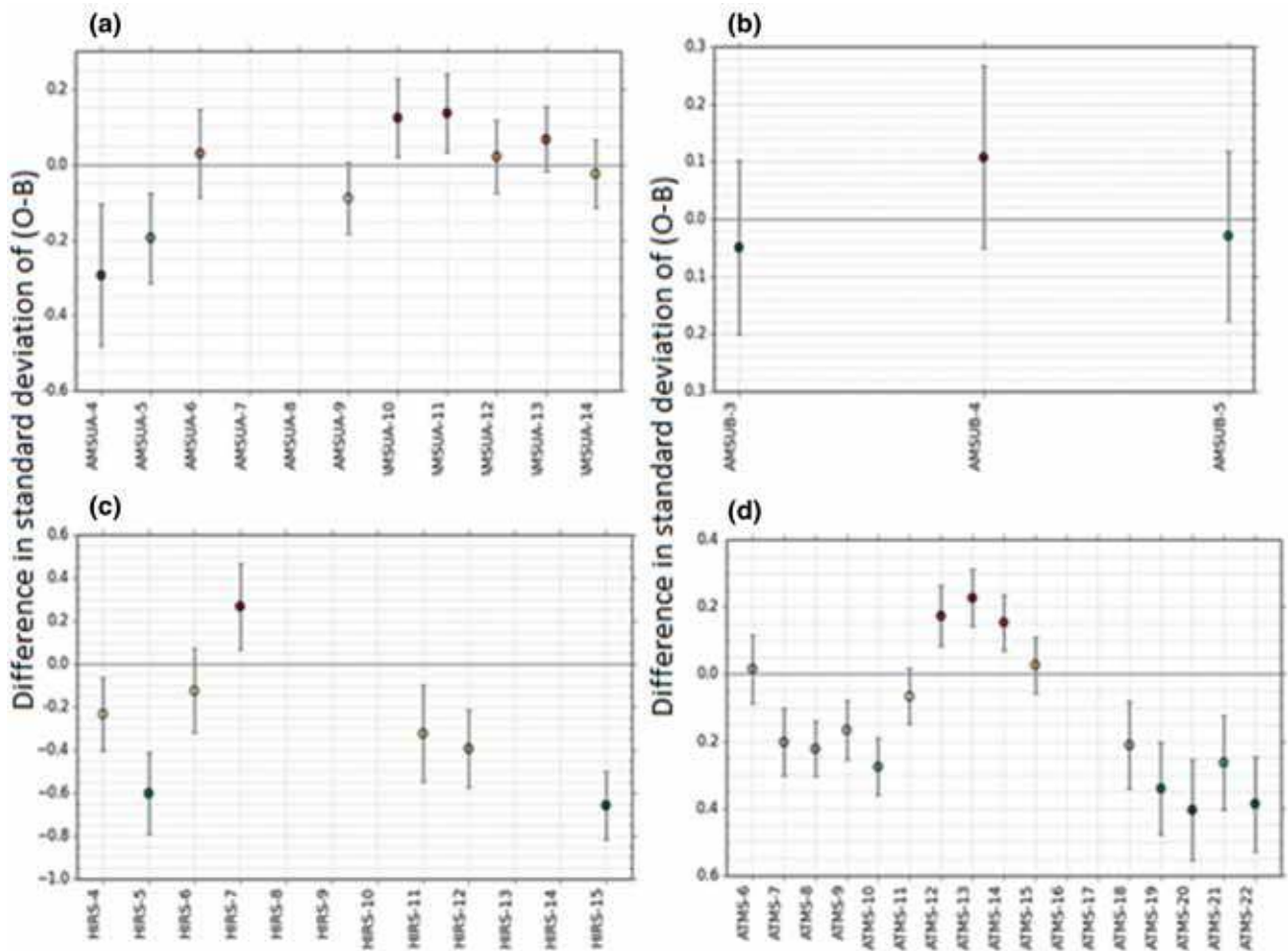
Figure 8. Impact of INSAT-3D WV CSBT assimilation on brightness temperatures from other instruments assimilated in the NCUM assimilation system. Difference in standard deviation of O–B between two experiments EXP and CNTL for (**a**) AMSUA from MetOp-1, (**b**) AMSUB from MetOp-1, (**c**) HIRS from MetOp-1 and (**d**) ATMS from NPP.

observations operationally being assimilated in NCUM except the INSAT-3D sounder and MVIRI. Since the INSAT-3D sounder and MVIRI have the same geographical coverage area, to see the impact of INSAT-3D imager WV radiances, these two observation types were excluded from both experiments. CNTL is the baseline experiment and table 1 shows the observations assimilated. The second experiment, EXP, assimilates all the observations in the baseline experiment along with INSAT-3D imager CSBTs. Both the experiments were run for the same period, 1–15 February 2017.

Before analysing the forecasts from the two experiments, it is important to see the impact of the newly introduced data on other radiances from different satellite instruments assimilated in the two experiments. The impact of INSAT-3D imager WV CSBT assimilation on other radiances is calculated in terms of the difference in the standard

deviation of the O–B of brightness temperatures of different instruments/channels between the two experiments. Although the impact is clear in most of the assimilated radiances from polar satellite instruments, for brevity only the plots of advanced microwave sounding unit-A (AMSU-A), AMSU-B and high resolution infrared sounder (HIRS) from MetOp-1 satellite and advanced technology microwave sounder (ATMS) from Suomi National Polar orbiting Partnership (SNPP) satellite are shown here. Figure 8 shows the difference in standard deviation of O–B between EXP and CNTL experiment. A negative value (EXP-CNTL) of difference in standard deviation of O–B shows positive impact due to the assimilation of INSAT-3D imager WV CSBT, and a positive difference shows negative impact.

AMSU-A has 15 channels in the microwave spectral region to probe the atmosphere particularly for the temperature information. Out of these
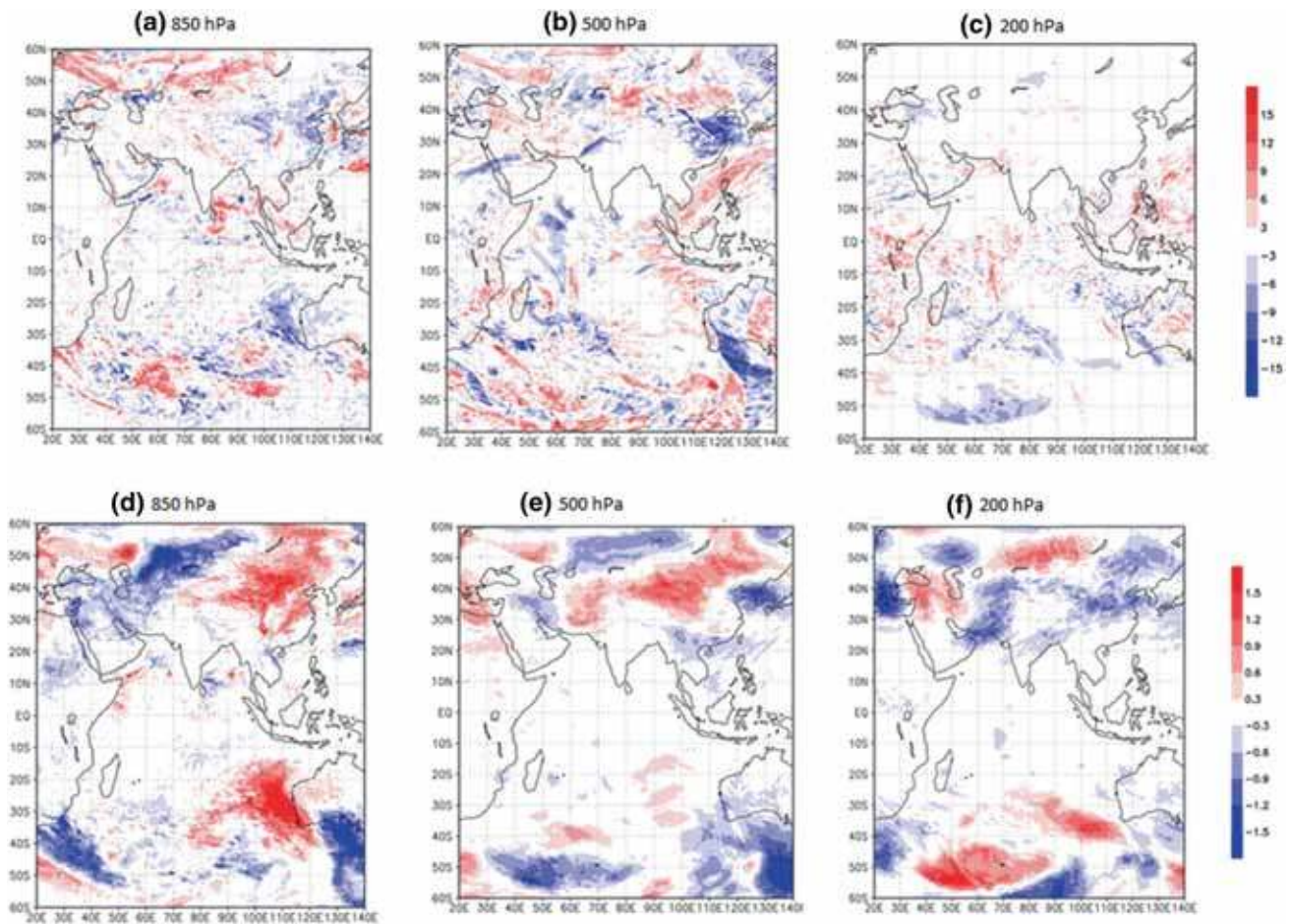
Figure 9. Day-1 forecast difference between EXP and CNTL, relative humidity (%) in the upper panel (at (**a**) 850 hPa, (**b**) 500 hPa, and (**c**) 200 hPa), and temperature (K) in the lower panel (at (**d**) 850 hPa, (**e**) 500 hPa and (**f**) 200 hPa).

15 channels, nine channels (4, 5, 6, 9, 10, 11, 12, 13, 14) are assimilated in the NCUM assimilation system. It can be seen from figure 8(a) that AMSU-A channels 4, 5 and 9 were positively influenced by the assimilation of INSAT-3D imager WV CSBTs. Other AMSU-A assimilated channels showed a slightly positive values. Similarly figure 8(b) is the AMSU-B, which has five channels in the microwave spectral region, provides information on atmospheric humidity. Out of these five AMSU-B channels, three channels (3, 4, 5) are assimilated in the NCUM system. AMSU-B channels 3 and 5 show positive impact due to the assimilation of INSAT-3D imager WV CSBTs, whereas channel 4 shows negative impact. HIRS has 20 channels out of which one is in the visible range and other 19 are in the IR spectral region. Out of these 19 channels, seven channels (4, 5, 6, 7, 11, 12, 15) are assimilated in the NCUM system. From figure 8(c), it can be seen that except channel 7, all the HIRS assimilated channels showed positive

impact due to the assimilation of INSAT-3D imager WV CSBT.

Figure 8(d) is the difference in standard deviation of O–B between the EXP and CNTL experiment for the brightness temperatures from ATMS onboard SNPP satellite. ATMS has 22 channels in the microwave region of the spectrum. Out of these 22 channels, the first 17 channels provide atmospheric temperature information, while the last 5 channels provide atmospheric humidity information. Channels 6–15 and 18–22 are assimilated in the NCUM system. All the humidity sensitive channels (18–22) show positive impact due to the assimilation of the INSAT-3D imager WV CSBTs. This could be because the moisture information from the INSAT-3D imager WV channel might have altered the analysis and hence decreased the standard deviation of ATMS humidity channel observations. Most of the ATMS temperature channels also showed positive impact as can be seen from figure 8(d). The
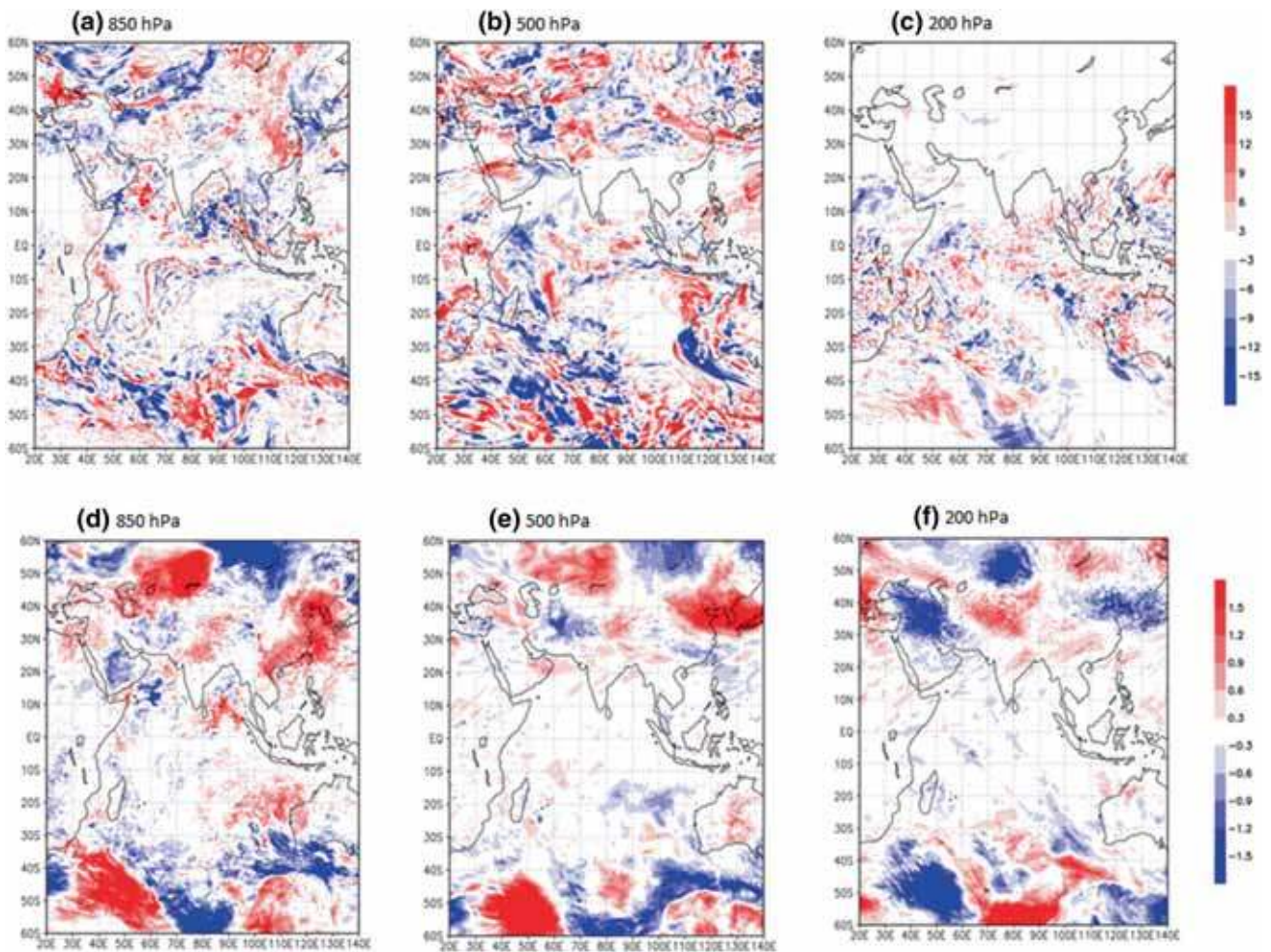
Figure 10. Day-3 forecast difference between EXP and CNTL, relative humidity (%) in the upper panel (at (**a**) 850 hPa, (**b**) 500 hPa and (**c**) 200 hPa), and temperature (K) in the lower panel (at (**d**) 850 hPa, (**e**) 500 hPa and (**f**) 200 hPa).

impact of the INSAT-3D imager WV CSBT is evident in radiances assimilated to the NCUM system from other satellite instruments, and hence in the NCUM assimilation system.

To see the impact of the INSAT-3D imager WV CSBTs in the forecast system, the average difference in forecast fields of temperature, humidity and winds between EXP and CNTL for the study period is generated for day 1 and day 3. Even though the humidity is significantly low at higher levels, the single observation experiments showed some influence of INSAT-3D imager WV CSBT assimilation at these regions. To support this, the spatial plot of humidity at 200 hPa is included in this section. Figure 9 shows the day-1 difference in forecasts between EXP and CNTL at different pressure levels, 850, 500 and 200 hPa, centred over the coverage area of INSAT-3D. The upper panel in figure 9 is for relative humidity and the lower panel represents temperature. Figure 9 shows

mixed impacts of INSAT-3D imager WV CSBT assimilation in the day-1 forecast fields of relative humidity and temperature. A moist bias is observed over the Bay of Bengal and some parts of the Arabian Sea at 850 hPa (figure 9a). Complementing the moistening effect at 850 hPa, due to the INSAT-3D imager WV CSBT assimilation, EXP forecasted a cold temperature (figure 9d). Thus, the assimilation of INSAT-3D imager WV CSBTs produced a cold and moist atmosphere in the lower levels. This behaviour is consistent with the results obtained from the single observation experiments (figures 4b and 5b). A dry bias is observed over some parts of the Arabian Sea at 500 hPa (figure 9b). At 200 hPa, the impact of INSAT-3D imager WV CSBT assimilation over the tropics is less both in relative humidity and temperature (figure 9c and f). From figure 9, it can be noticed that WV CSBT assimilation has a larger impact in the humidity forecasts, but a
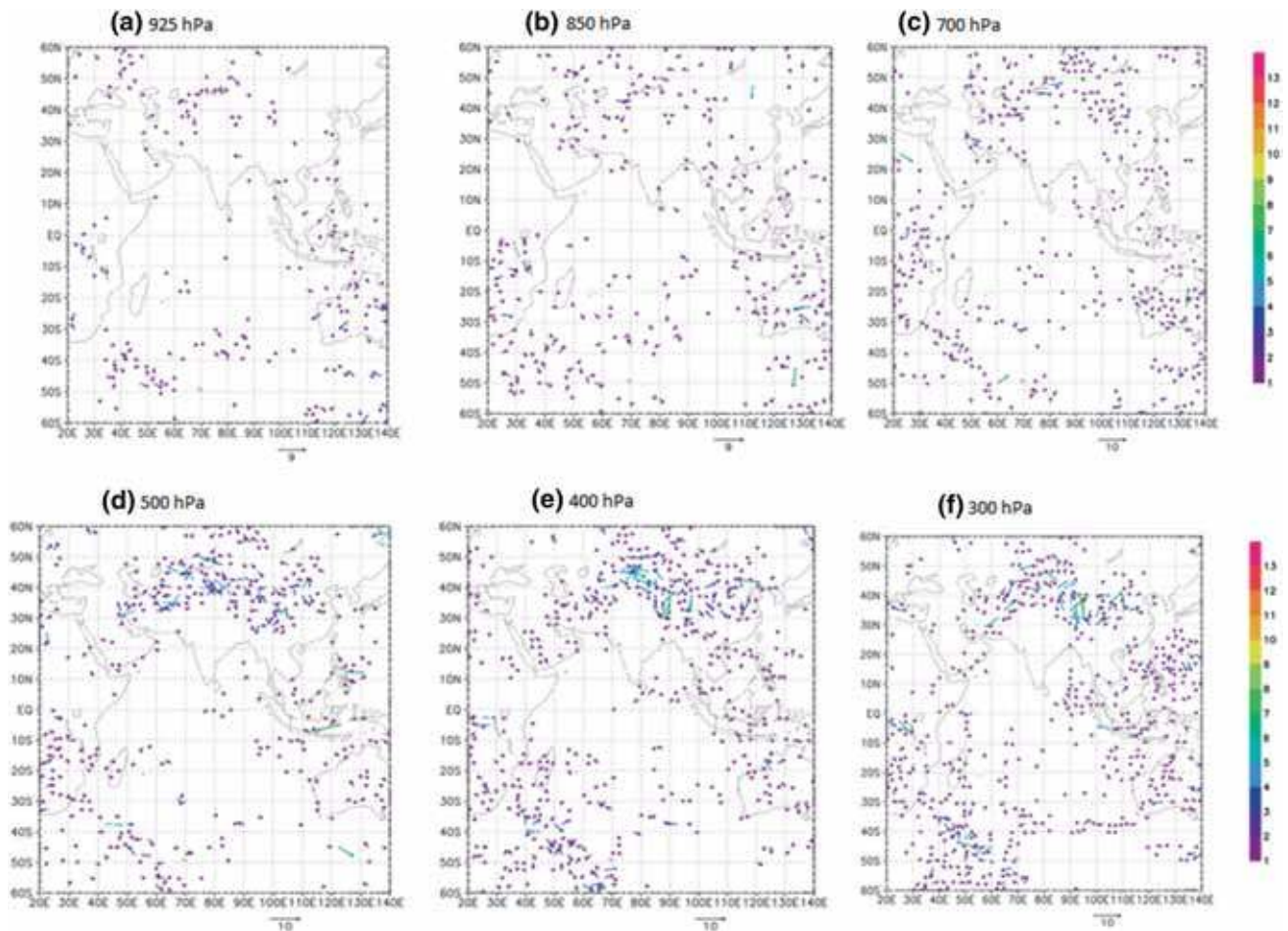
Figure 11. Day-1 forecast difference in wind vectors between EXP and CNTL at different model levels: (**a**) 925 hPa, (**b**) 850 hPa, (**c**) 700 hPa, (**d**) 500 hPa, (**e**) 400 hPa and (**f**) 300 hPa.

smaller impact in the temperature forecasts, particularly, over the tropics. This can be attributed mainly to the fact that the WV channel provides humidity information rather than temperature information. This is again confirmed with the validation of model forecast variables with respect to the unbiased in situ radiosonde observations described in section 5.3. However, while observing the plots, although the impact for temperature is minimal over the tropics, noticeable impact is seen north of the tropics as compared to that in humidity. This can be attributed to the flow-dependent features of analysis increment variables as depicted in the spatial plots of analysis increment in potential temperature (figure 6) from the single observation experiment.

Figure 10 is similar to figure 9, but for day-3 forecasts. A moist bias over the Arabian Sea and a dry bias over the Bay of Bengal are observed (figure 10a) in the day-3 forecast and complementing the relative humidity, the temperature

forecasts show a cold bias over the Arabian Sea and a warm bias over the Bay of Bengal (figure 10d). In the higher levels, the assimilation impact is observed to be neutral over India and the surrounding oceanic regions. Similar to day-1 forecasts (figure 9), the day-3 forecasts also showed higher impact of WV CSBT in the humidity fields, and over the tropics, the impact on the temperature forecast is neutral.

Figure 11 shows the day-1 differences in the vector wind forecasts between EXP and CNTL at different levels. In figure 11, the upper panels show the wind vector difference at lower levels, at 925 hPa (figure 11a), 850 hPa (figure 11b) and 700 hPa (figure 11c). In day-1 forecast, the wind vector differences are less than 1 m/s in the lower levels. The lower panel of figure 11 shows the day-1 wind vector differences at higher levels, 500 hPa (figure 11d), 400 hPa (figure 11e) and 300 hPa (figure 11f). In contrast to the lower levels, the upper levels show a vector difference of 7 m/s in the EXP, confirming the
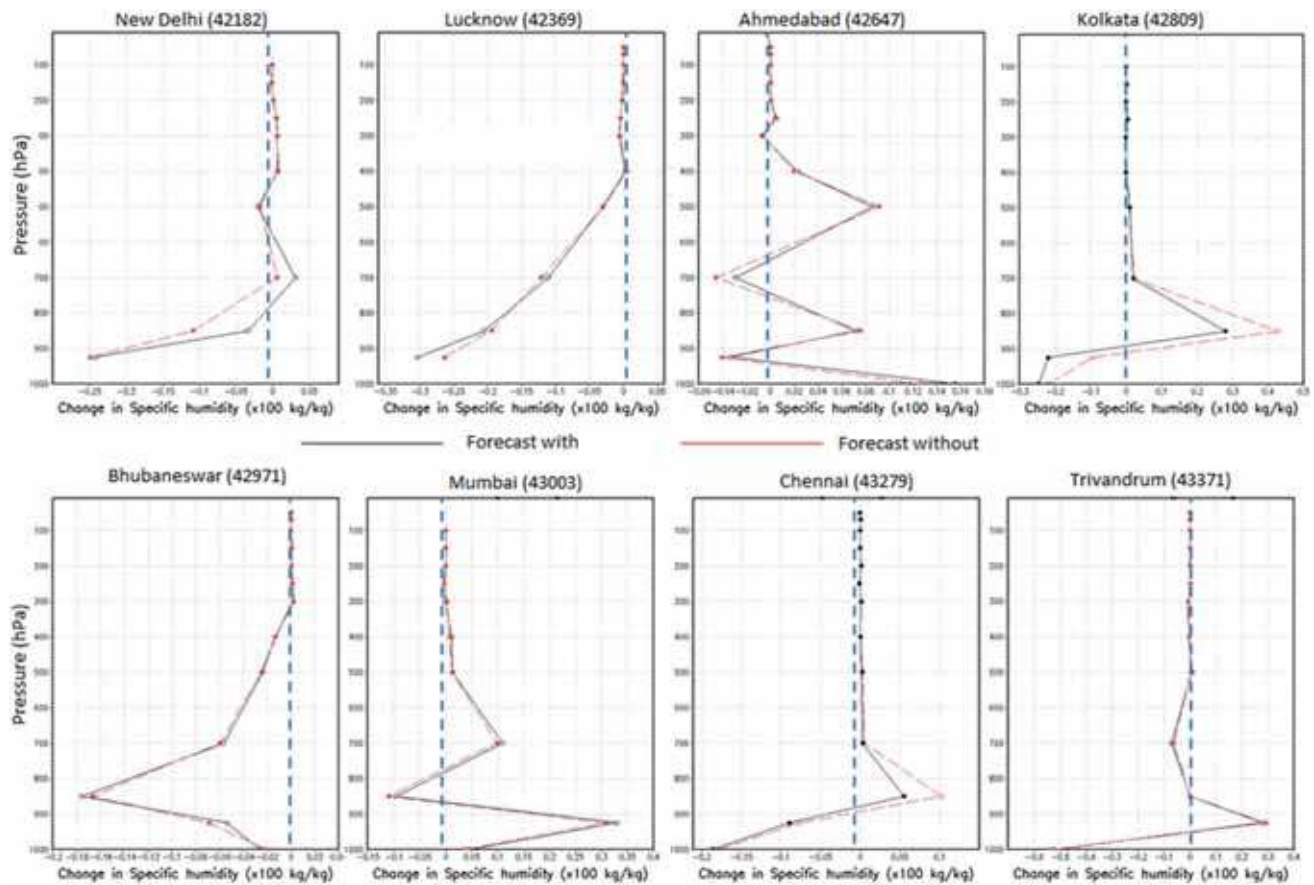
Figure 12. Validation of model forecasted specific humidity (kg/kg) with RS observations at different locations. Black and red curves, respectively, represent the forecast–observation (F–O) from EXP and CNTL. (X-axis scale factor: multiplied by 100).

influence of WV CSBT assimilation in the upper-level wind forecasts. WV CSBTs complement cloudy WV winds at higher levels. Most of the time the height assignment of clear sky WV winds is difcult since under clear sky conditions radiation in the WV channel is emitted from a deep atmosphere (Velden *et al.* 1997).

5.3 *Comparison of forecasts with in situ observations*

A new observation type, INSAT-3D imager CSBTs, is introduced in the NCUM assimilation system, and the single observation experiments and global assimilation experiments show the influence of this new observation type in the analysis increment of different model parameters as well as in the model prognostic and diagnostic variables. To assess whether this influence is positive or negative, it is mandatory to compare the forecast variables with that of observations. In situ observations like radiosondes (RS) are a

good source of independent and unbiased observations. RS observations from different locations over India are considered for validation. Eight different World Meteorological Organisation (WMO) RS stations (WMO-ID), viz., New Delhi (42,182), Lucknow (42,639), Ahmedabad (42,647), Kolkata (42,809), Bhubaneswar (42,971), Mumbai (43,003), Chennai (43,279) and Trivandrum (43,371) are considered for the validation of meteorological parameters from the two experiments EXP and CNTL.

Figures 12–14 are the profiles of forecast–observation (F–O) plots of different parameters like specific humidity (kg/kg), temperature (K) and zonal wind speed (m/s) from the two experiments EXP and CNTL. Figure 12 shows the difference in the forecasted specific humidity with respect to the RS observations over the eight different locations. In figure 12, the black curve represents the difference between the model forecasted specific humidity from EXP and RS observations, while the red curve shows the same for CNTL. Figures 13 and 14 are in similar line to figure 12,
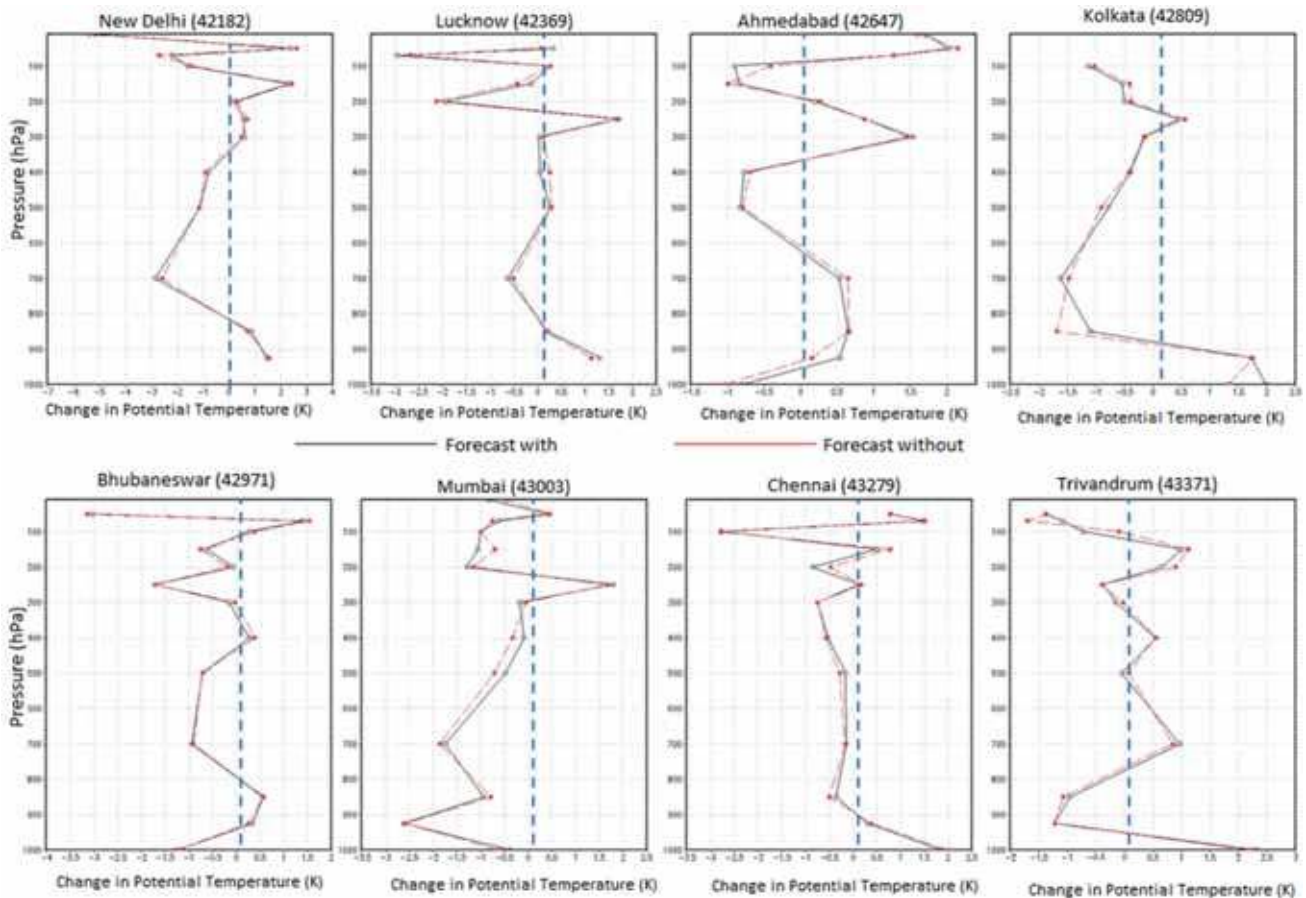
Figure 13. Validation of model forecasted potential temperature (K) RS observations at different locations. Black and red curves, respectively, represent the forecast–observation (F–O) from EXP and CNTL.

but for the variables temperature and zonal wind speed.

From figure 12, the F–O plots of the specific humidity profiles from EXP (experiment with INSAT-3D imager CSBTs included) are closer to the observations approximately from 850 to 400 hPa compared to the same from the CNTL at about six locations, Lucknow, Ahmedabad, Kolkata, Bhubaneswar, Chennai and Trivandrum. New Delhi and Mumbai are depicting slightly higher values of F–O from the EXP. In general, the validation of model forecasted specific humidity with RS observations shows the assimilation of INSAT-3D imager CSBTs has a positive impact in the humidity field. As the presence of humidity is significantly low in the upper levels, both EXP and CNTL show the same values of F–O, with almost zero difference.

The F–O plots of potential temperature profiles from the two experiments at eight different locations are shown in figure 13. The trend that is observed in the specific humidity forecast is not seen in the potential temperature forecast. At some locations, F–O of potential temperature from EXP (Kolkata, Mumbai, Chennai, Trivandrum) is better, and at some other locations, F–O of potential temperature from CNTL (New Delhi, Lucknow, Ahmedabad) is better. There are some locations (Bhubaneswar) where both EXP and CNTL exactly match. The influence of INSAT-3D imager CSBT assimilation does not have a marked influence on the temperature field compared to the humidity field. Figure 14 shows the F–O plots of the zonal wind component profiles at the eight selected locations. At most of the locations, F–O from EXP is less than that from CNTL. In general, the wind also shows a positive impact due to the assimilation of the INSAT-3D imager CSBTs at most of the locations. The validation of model forecast fields with respect to the independent RS observations shows that the assimilation of INSAT-3D imager CSBTs has a positive impact on the humidity and wind fields, whereas the impact on the temperature field is comparatively small.
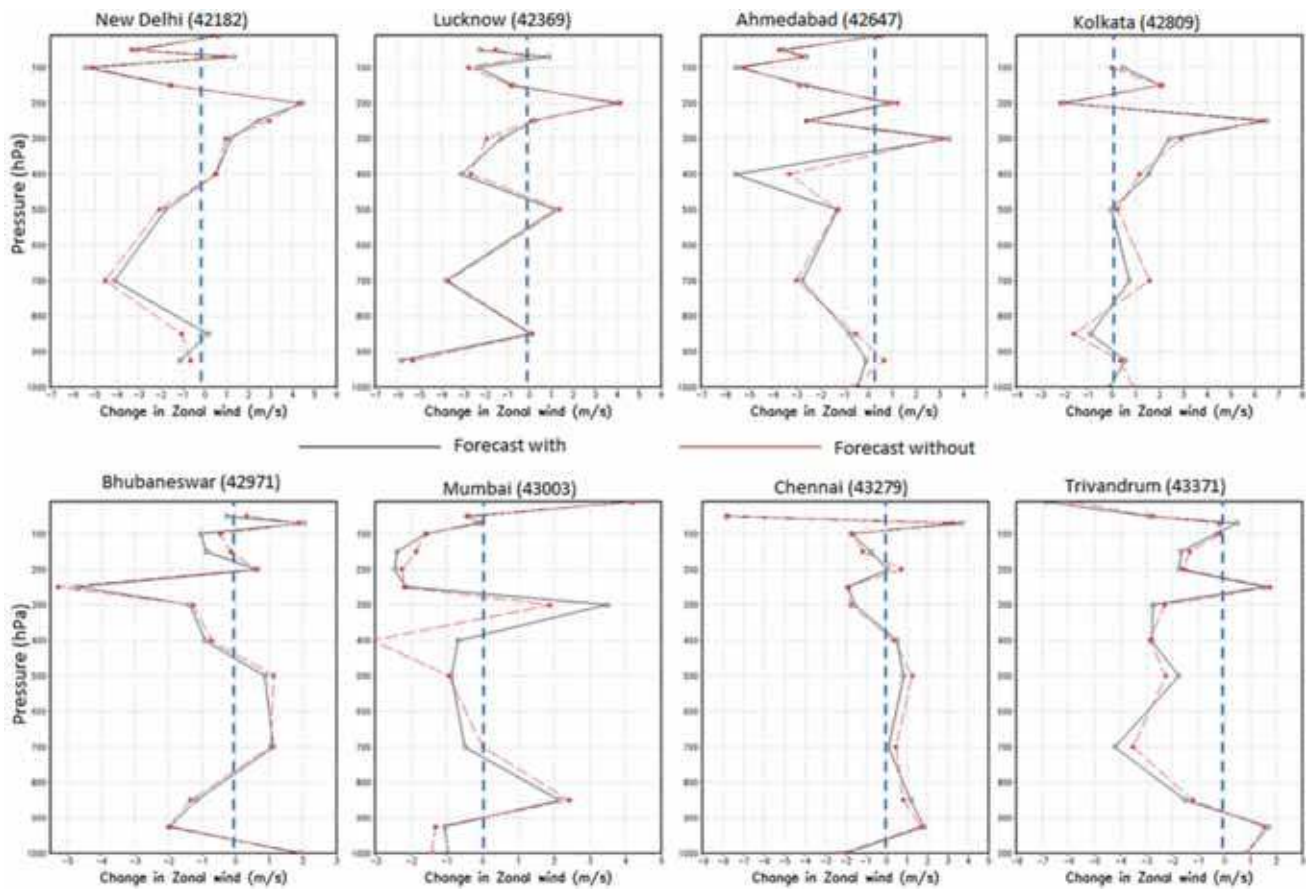
Figure 14. Validation of model forecasted zonal wind (m/s) with RS observations at different locations. Black and red curves, respectively, represent the forecast–observation (F–O) from EXP and CNTL.

6. Conclusions

INSAT-3D imager WV CSBTs were assimilated in the NCUM assimilation and forecast model. Before assimilation, the observed CSBTs were bias corrected using model simulated CSBTs. A bias of 2–3 K was found in the observed WV CSBTs with respect to the model background. Bias corrected CSBTs have been assimilated operationally in the NCUM system since August 2018. The impact of INSAT-3D imager WV CSBTs was analysed through a series of single observation experiments and global assimilation experiments. The single observation experiments show that INSAT-3D imager WV and MVIRI WV channels have a similar influence on the analysis increment of both theta and specific humidity. The specific humidity increments are mainly driven by the sounder in the assimilation system, but the imager modifies them. Global assimilation experiments also support the single observation experimental results. The influence of INSAT-3D CSBTs was observed mainly in the humidity field and the upper tropospheric winds. The impact on the temperature field is neutral in the tropics. Validation of forecast fields with respect to the in situ radiosonde profiles showed that the assimilation of INSAT-3D imager WV CSBT positively affects the humidity and wind fields.

References

Auligne T, McNally A P and Dee D P 2007 Adaptive bias correction for satellite data in a numerical weather prediction system; *Quart. J. Roy. Metereol. Soc.* **133** 631–642, https://doi.org/10.1002/qj.56.

Bell W, English S J, Candy B, Atkinson N, Hilton F, Baker N, Swadley S D, Campbell W F, Bormann N, Kelly G and Kazumori M 2008 The assimilation of SSMIS radiances in numerical weather prediction models; *IEEE Trans. Geosci. Remote Sens.* **46**(**4**) 884–900.

Clayton A M, Lorenc A C and Barker D M 2013 Operational implementation of a hybrid ensemble/4D-Var global data assimilation system at the Met office; *Quart. J. Roy. Metereol. Soc.* **139** 1445–1461, https://doi.org/10.1002/qj.2054.

Das Gupta M, Priti S and Rani S I 2015 Validation of INSAT-3D atmospheric motion vectors; NMRF/RR/01/2015, 27p.

Deb S K, Kumar P, Kiran Kumar A S, Pal P K, Kaushik N and Sangar G 2015 Atmospheric motion vectors from INSAT-3D: Initial quality assessment and its impact on track forecast of cyclonic storm Nanauk; *Atmos. Res.* **169** 1–16, https://doi.org/10.1016/j.atmosres.2015.09.010.

Doherty A, Atkinson N, Bell W and Smith A 2015 An assessment of data from the advanced technology microwave sounder at the Met office; *Adv. Meteorol.* **2015** 1–16, Article ID 956920, http://dx.doi.org/10.1155/2015/956920.

George J P, Rani S I, Jayakumar A, Mohandas S, Mallick S, Lodh A, Rakhi R, Sreevathsa M N R and Rajagopal E N 2016 NCUM data assimilation system; NMRF/TR/01/2016, 20p.

HarrisB and Kelly G 2001 A satellite radiance bias correction scheme for data assimilation; *Quart. J. Roy. Meteorol. Soc.* **127** 1453–1468.

Honda T, Miyoshi T, Lien G, Nishizawa S, Yoshid R, Adachi SA, Terasaki K, Okamoto K, Tomita H and Bessho K 2018 Assimilating all-sky Himawari-8 satellite radiances: A case of Typhoon Soudelor (2015); *Mon. Weather Rev.* **146** 213–229, https://doi.org/10.1175/mwr-d-16-0357.1.

Kelkar R R 2019 Satellite meteorology in India: Its beginning, growth and future; *Mausam* **70**(**1**) 1–14.

Kopken C, Kelly G and Thepaut J N 2004 Assimilation of Meteosat radiance data within the 4D-Var system at ECMWF: Assimilation experiments and forecast model; *Quart. J. Roy. Meteorol. Soc.* **130** 2277–2292.

Kumar P, Deb S K, Kishtawal C M and Pal P K 2016 Impact of assimilation of INSAT-3D retrieved atmospheric motion vectors on short-range forecast of summer monsoon 2014 over the south Asian region; *Theor. Appl. Climatol.*, https://doi.org/10.1007/s00704-015-1722-5.

Kumar S, Rani S I, George J P and Rajagopal E N 2018 Megha-tropiques SAPHIR radiances in a hybrid 4D-Var data assimilation system: Study of forecast impact; *Quart. J. Roy. Meteorol. Soc.*, https://doi.org/10.1002/qj.3251.

Kurzrock F, Cros S, Ming F C, Otkin J A, Hutt A, Linguet L, Lajoie G and Potthast R 2018 A review of the use of geostationary satellite observations in regional-scale models for short-term cloud forecasting; *Meteorol. Z.* **27**(**4**) 277–298.

Lorenc A C 2003a Modelling of error covariances by four dimensional variational data assimilation; *Quart. J. Roy. Metereol. Soc.* **129** 3167–3182, https://doi.org/10.1256/qj.02.131.

Lorenc A C 2003b The potential of the ensemble Kalman filter for NWP: A comparison with 4D-Var; *Quart. J. Roy. Metereol. Soc.* **129** 3183–3203, https://doi.org/10.1256/qj.02.132.

Lorenc A C, Bowler N, Clayton A M, Pring A R and Fairbairn D 2015 Comparison of hybrid-4DEnVar and hybrid-4DVar data assimilation methods for global NWP; *Mon. Weather Rev.* (*Sixth WMO data assimilation symposium special collection*), https://doi.org/10.1175/MWR-D-14-00195.1.

Lu Q, Bell W, Bauer P, Bormann N and Peubey C 2011 Characterizing the *FY-3A* microwave temperature sounder using the ECMWF model; *J. Atmos. Ocean Tech.* **28**(**11**) 1373–1389.

Munro R, Kopken C, Kelly G, Thepaut J N and Saunders R 2004 Assimilation of Meteosat radiance data within the 4D-Var system at ECMWF: Data quality monitoring, bias correction and single cycle experiments; *Quart. J. Roy. Metereol. Soc.* **130** 2293–2313.

Prasad V S 2012 Conversion of NCEP decoded data to UK MET office Obstore format; NCMR/OB/1/2012.

Prasad V S 2014 Satellite data processing for NCMRWF unified model (NCUM); NMRF/RR/2/2014.

Prasad V S and Rani S I 2014 Data pre-processing for NCMRWF unified model (NCUM): Version 2; NMRF/RR/01/2014, 19p.

Rabier F 2005 Overview of global data assimilation developments in numerical weather-prediction centres; *Quart. J. Roy. Metereol. Soc.* **131** 3215–3233, https://doi.org/10.1256/qj.05.129.

Rawlins F, Ballard S P, Bovis K J, Clayton A M, Li D, Inverarity G W, Lorenc A C and Payne T J 2007 The Met office global 4-dimensional variational data assimilation system; *Quart. J. Roy. Metereol. Soc.* **133** 347–362, https://doi.org/10.1002/qj.32.

Rajagopal E N, Iyengar G R, George J P, Das Gupta M, Mohandas S, Siddharth R, Gupta A, Chourasia M, Prasad V S, Aditi S K and Ashish A 2012 Implementation of the UM model based analysis – Forecast system at NCMRWF; NMRF/TR/2012, 45p.

Rani S I and Prasad V S 2013 Simulation and Validation of INSAT-3D Sounder Data at NCMRWF; https://cimss.ssec.wisc.edu/itwg/itsc/itsc19/program/papers/1_08_rani.pdf.

Rani S I and Das Gupta M 2014 An inter-comparison of Kalpana-1 and Meteosat-7 atmospheric motion vectors against radiosonde winds and NWP forecasts during monsoon 2011; *Meteorol. Appl.* **21** 820–830, https://doi.org/10.1002/met.1411.

Rani S I, Taylor R, George J P and Rajagopal E N 2016 Use of INSAT-3D sounder and imager radiances in the 4D-VAR data assimilation system and its implications in the analyses and forecasts; *Proc. SPIE* **9876** 98761G-1, https://doi.org/10.1117/12.2223496.

Rao P A, Velden C S and Braun S A 2002 The vertical error characteristics of GOES-derived winds: Description and experiments with numerical weather prediction; *J. Appl. Meteorol.* **41** 253–271.

Saunders R, Matricardi M, Geer A, Rayer P, Embury O and Merchant C 2010 RTTOV9 science and validation plan; NWPSAF-MO-TV-020, 2010, http://nwpsaf.eu/oldsite/deliverables/rtm/rttov9_files/rttov9_svr.pdf.

Sharma P, Rani S I and Das Gupta M 2016 Validation of INSAT-3D atmospheric motion vectors for monsoon 2015; *Proc. SPIE* **9881** 988125-1, https://doi.org/10.1117/12.2223564.

Singh R, Pal P K and Joshi P C 2010 Assimilation of Kalpana very high resolution radiometer water vapor channel radiances into a mesoscale model; *J. Geophys. Res.* **115** D18124, https://doi.org/10.1029/2010jd014027.

Singh R, Ojha SP, Kishtawal CM, Pal PK and Kiran Kumar AS 2016 Impact of the assimilation of INSAT-3D radiances on short-range weather forecasts; *Quart. J. Roy. Metereol. Soc.* **142** 120–131.

Stengel M 2008 *Assimilation of SEVIRI's Water Vapour Channel Observations in Clear-Sky Conditions into the HIRLAM Model*; Technical Report No. 68.

Szyndel M D E, Thepaut J N and Kelly G 2005 Evaluation of potential benefit of SEVIRI water vapour radiance data from Meteosat-8 into global numerical weather prediction analyses; *Atmos. Sci. Lett.* **6** 105–111.

Thepaut J N 2003 Satellite data assimilation in numerical weather prediction: An overview; In: *Proceedings of ECMWF Seminar on Recent Developments in Data Assimilation for Atmosphere and Ocean*, ECMWF, Reading, UK, 8–12 September 2003, pp. 75–96.

Trigo I F and Viterbo P 2003 Clear-sky window channel radiances: A comparison between observations and the ECMWF model; *J. Appl. Meteorol.* **42** 1463–1479.

Velden C S, Niemann S J, Menzel W P and Wanzong S T 1997 Upper tropospheric winds derived from geostationary satellite water vapour observations; *Bull. Am. Meteorol. Soc.* **78** 173–195.

Yang C, Liuz Z, Gao F, Child PP and Min J 2017 Impact of assimilation goes imager clear-sky radiance with a rapid refresh assimilation system for convection-permitting forecast over Mexico; *J. Geophys. Res.: Atmos.* **122** 5472–5490. https://doi.org/10.1002/2016jd026436.

Corresponding editor: KAVIRAJAN RAJENDONEDRAN